Bulletin of Engineering Geology and the Environment (2022) 81:221
https://doi.org/10.1007/s10064-022-02712-0

ORIGINAL PAPER

Hydraulic properties of ignimbrites: matrix and fracture permeabilities in two pyroclastic flow deposits from Cimino-Vico volcanoes (Italy)

Vincenzo Allocca[1] · Pasquale Colantuono[1] · Abner Colella[1] · Simone M. Piacentini[2] · Vincenzo Piscopo[2]

Received: 3 November 2021 / Accepted: 19 April 2022

Abstract

Hydrological properties of ignimbrites are known in detail only for some areas, although these rocks cover large areas with considerable thicknesses in many volcanic regions of the world. This study investigates hydrological properties of two ignimbrites of Latium (Central Italy), different in age, composition, and origin. The dual porosity of the ignimbrites was examined through laboratory tests, pumping tests, and outcrop surveys. The degree of welding, composition, and stratigraphy of the two ignimbrites are the main factors determining their hydrological properties. The two ignimbrites share a low matrix permeability, showing a different fracturing degree. The more welded ignimbrite is characterized by lower porosity of the matrix and higher fracturing degree, while the less welded ignimbrite is characterized by higher porosity of the matrix and lower fracturing degree. Hydraulic conductivity and storage capacity of the highly welded ignimbrite mainly depend on the denser network of discontinuities. The hydraulic conductivity of the younger ignimbrite, less welded, mainly depend on the sparser network of discontinuities and on the layer of unconsolidated coarse pyroclastic deposits at its base, while the storage capacity depends on the more porous matrix. Should the pyroclastic rocks be used as aquifer for water supplies, or, in other cases, as substratum of waste disposal sites, the dual porosity of the ignimbrites must necessarily include different scales of analysis in order to evaluate the role of matrix and fractures on the permeability of rock mass. In any case, the results of laboratory and on-site tests are to be interpreted taking into account the stratigraphy of the ignimbrite.

Keywords Ignimbrite · Hydraulic conductivity · Dual porosity · Fractured rock · Cimino-Vico volcanoes

Introduction

Ignimbrites, deposits formed by the emplacement of pyroclastic flows whether welded or unwelded (Sparks et al. 1973; Fisher and Schmincke 1984), cover large areas with considerable thicknesses in many volcanic regions of the world, such as Western United States, Mexico, Central America, Japan, New Zealand, Iceland, and Southern Europe. Despite their wide diffusion, hydrological properties of these rocks are known in detail only for some areas (Winograd 1971; Istok et al. 1994; Foster et al. 1985; Fuller and Sharp 1992; Sharp et al. 1993; Flint and Selker 2003; Smyth and Sharp 2006). As a matter of fact, hydrological knowledge of ignimbrites is fundamental, since pyroclastic flow deposits constitute aquifers used for extraction of groundwater and substrata for hosting waste disposal sites in many regions around the world.

A large portion of the literature focuses on matrix porosity and permeability of ash flow tuffs with different degree of welding (e.g., Flint 1998; Istok et al. 1994; Flint and Selker 2003). Few studies examine the permeability on the whole, including permeability due to primary porosity of the matrix and permeability due to secondary porosity of the fractures. The role of the dual porosity of tuffs is evidenced by studies conducted in the tuffs of Yucca Mountain (Nevada) (e.g., Peters and Klavetter 1988). Sharp et al. (1993) based on laboratory tests and geological surveys on ash flow tuffs highlight that the matrix permeability depends on the degree of welding and weathering; the same authors argue that fracture density and permeability are greater in more densely welded tuffs.

✉ Vincenzo Piscopo
piscopo@unitus.it

[1] Dipartimento di Scienze della Terra, dell'Ambiente e delle Risorse, Università degli Studi di Napoli Federico II, Naples, Italy

[2] Dipartimento di Scienze Ecologiche e Biologiche, Università degli Studi della Tuscia, Viterbo, Italy

Published online: 04 May 2022

Smyth and Sharp (2006) report one of the most comprehensive research on the hydrological properties of these rocks. The authors analyze extensive hydrological data related to ash flow tuffs, combining new knowledge with the previously acquired information. Laboratory and in situ data (pumping, injection, slug, and tracer tests) derive primarily from Yucca Mountain Tuffs and secondarily from tuffs located elsewhere (Texas, Arizona, New Mexico, Mexico, Costa Rica, and Indonesia). The results of the study show that hydrological proprieties of ash flow tuffs vary greatly depending on degree of welding, cooling rate, mineralogical alteration products, fracturing degree, and post-depositional tectonic stress. The quoted authors and other researchers (e.g., Lahoud et al. 1984; Rasmussen et al. 1993; Flint and Selker 2003) found a wide variation in porosity (2–60%) and hydraulic conductivity (10^{-14}–10^{-4} m/s) due to matrix and fracture heterogeneity. The highest hydraulic conductivity values are derived from pumping tests. Said values are greater by several orders of magnitude than those measured in laboratories, since the volumes explored by in situ well tests include heterogeneity of tuff matrix and matrix plus fracture permeability (Smyth and Sharp 2006).

In Italy, the ignimbrites are widespread in the Pliocene–Quaternary volcanic regions (Peccerillo 2005). These rocks host aquifers used locally for water supply, are extracted in quarries as building material since Roman Times and sometimes represent the substratum of waste disposal sites. The few studies concerning the hydrological characterization of these rocks mainly regard the determination of porosity and permeability in laboratory (e.g., Ottaviani 1988; Vanorio et al. 2002; Peluso and Arienzo 2007; Heap et al. 2014; Montanaro et al. 2016; Carlino et al. 2018). A detailed study of the hydrological behavior of these ignimbrites, considering them a dual-porosity medium, has not been published to date.

In order to contribute to the knowledge of the hydrological properties of ignimbrites, our study examines two ignimbrites of Latium, Central Italy (Ignimbrite of the Cimino Volcano and C Ignimbrite of the Vico Volcano), different in age, composition, and origin. The purpose of this research is to evaluate hydraulic conductivity at different observation scales through laboratory tests, pumping tests, and outcrop surveys. Results obtained from the multiscale characterization of the two ignimbrites are discussed with a particular focus on the role of matrix permeability and fracture permeability in hydrological properties of rock mass.

Materials

The materials examined belong to two volcanic complexes in Central Italy: the Cimino Volcano and the Vico Volcano (Fig. 1a). These volcanoes are related to the Pliocene–Pleistocene magmatic activity developed along the Tyrrhenian margin of Italy. The Cimino Volcano was formed during 1.35–0.95 Ma, and its products are attributed to the potassic series (Tuscan Magmatic Province). The Vico Volcano erupted between 419 and 95 ka, and its products are attributed to the high-potassic series (Roman Magmatic Province) (Peccerillo and Manetti 1985; Conticelli and Peccerillo 1992; Perini et al. 1997; Peccerillo 2005).

The magmatic activity of the Cimino Volcano generated mainly lava domes, pyroclastic flows, and lava flows. The volcanic history of the Vico Volcano was more complex, including explosive Plinian-type activity, effusive activity with the formation of a strato-volcano, ignimbrite-forming eruptions and caldera genesis, and circum-caldera hydromagmatic and strombolian eruptions (Micheluccini et al. 1971; Locardi 1965; Sollevanti 1983; Bertagnini and Sbrana 1986; Lardini and Nappi 1987; Perini et al. 1997).

This study regards two of the most voluminous ignimbrites of these two volcanic complexes: the Cimino Ignimbrite of the Cimino Volcano (hereafter ICV) and the C Ignimbrite of the Vico Volcano (hereafter CIV).

The ICV, erupted 1.3 Ma, is trachytic in composition, covering an area of about 300 km^2 (Fig. 1b) with a volume of about 15 km^3 and variable thickness up to 150–200 m in the proximal zones. The ignimbrite is a massive gray, high-welded deposit, which grades into a pink, non-welded, pomiceous facies in the distal zones. The ash-size matrix contains sanidine, biotite, plagioclase, and pyroxene crystals. In the welded zone, flattened quartz-latitic pumice clasts and glassy fragments define a eutaxitic texture. Black *fiamme* and sparse lithic clasts of sedimentary and lava-dome fragments characterize the welded facies. The pyroclastic deposit consists of more overlapping flow units. The massive horizons are often characterized by vertical fissuring and pseudo-stratification. In the proximal zones, at the base of the welded facies, an agglomerate formed by blocks of ignimbrite and lava dome welded by a minute matrix is present (Lardini and Nappi 1987; Cimarelli and De Rita 2006).

The CIV is the most represented deposit of the Vico Volcano, covering an area of about 1250 km^2 (Fig. 1b); the volume of the formation has been estimated in about 10 km^3, and the thickness varies, starting from 10 m and up to 60–80 m. The deposit, erupted 151 ka is phonolitic in composition. The base of ignimbrite is constituted by a metric horizon of white Plinian pumices micro-vesiculated containing sanidine, pyroxene, and biotite. Three pumice flow units from decametric to metric thickness follow; the matrix consists of pale-gray ashes with rounded sub-aphyric pumices. A lag-breccia deposit follows, with scarce matrix and maximum thickness of 20 m in the proximal zones. Towards the distal zones, the matrix is constituted by coarse lapilli, and the thickness of the deposit decreases. Lithics are constituted by lavas, clay fragments, and thermo-metamorphic rocks. The

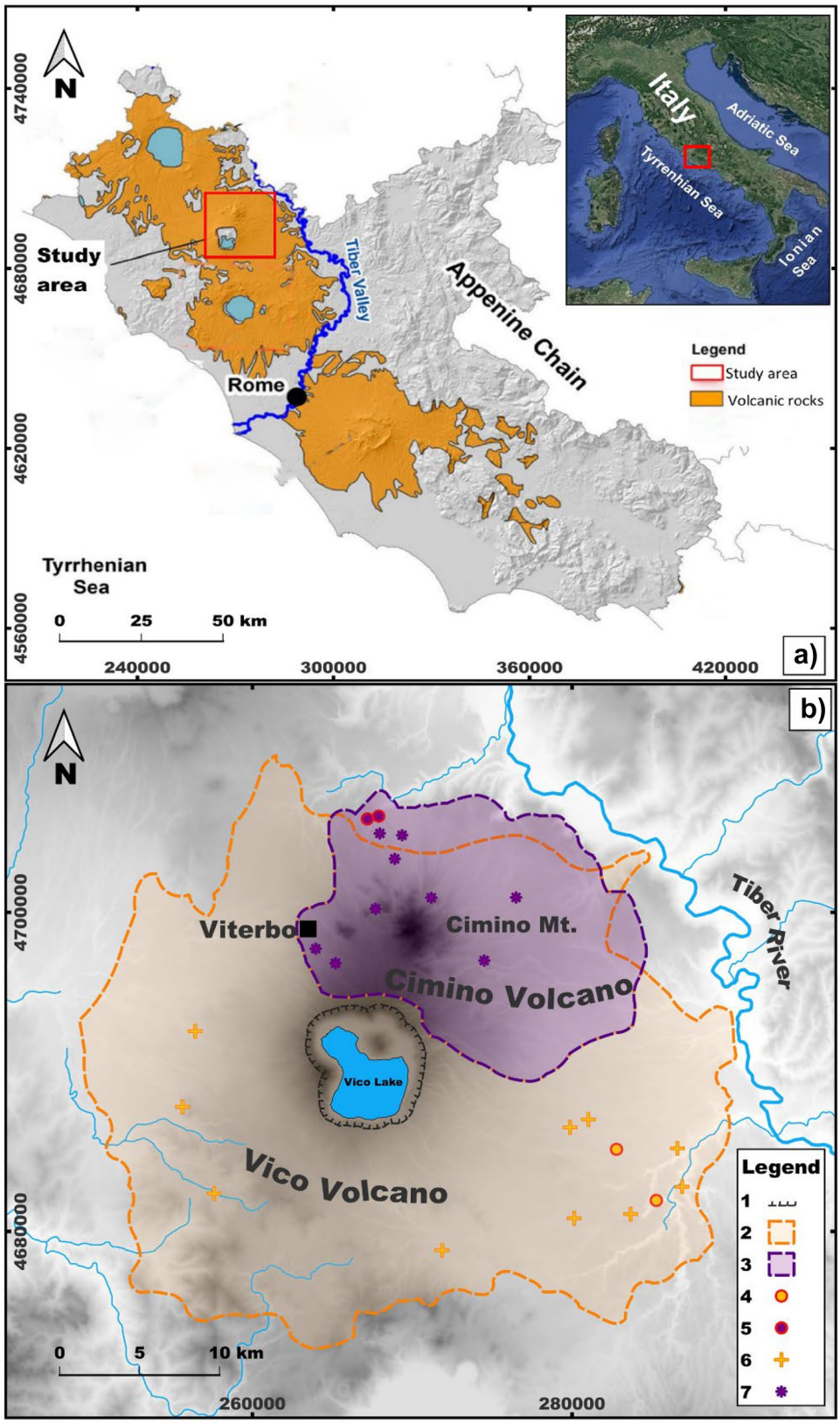

Fig. 1 **a** Location of Cimino-Vico volcanoes. **b** Distribution of ignimbrites studied in the Cimino-Vico volcanic area (modified from Nappi et al. 2004): 1, caldera rim; 2, boundary of C Ignimbrite (CIV); 3, boundary of Cimino Ignimbrite (ICV); 4, sampling site of the CIV; 5, sampling site of the ICV; 6, outcrop surveys of the CIV; 7, outcrop surveys of the ICV

sequence continues with a massive, welded deposit constituted by flattened scoriae, followed by a sillar-type deposit with a zeolitized matrix containing rare, gray-rounded pumices (Locardi 1965; Bertagnini and Sbrana 1986; Perini et al. 1997; Nappi et al. 2004).

The two ignimbrites were examined by means of field surveys, laboratory analyses, and on-site tests. Field surveys included the examination of several ignimbrite outcrops selected from natural escarpments, road cuts, and quarry fronts. The ICV examined in 9 outcrops (Fig. 1b) is fairly homogeneous in texture and massive throughout the entire thickness (up to several tens of meters). The pyroclastic deposit appears highly welded with a typical eutaxitic texture, black *fiamme*, and sparse lithic clasts. Frequent vertical and less frequent sub-horizontal discontinuities cross the outcrops (Fig. 2a).

The CIV was examined in 11 outcrops (Fig. 1b). The outcropping facies with greater thickness (up to some tens of meters) is represented by a welded and homogeneous deposit composed mainly of pumices (up to the centimeter size) in a fine ash matrix. Black scoriae (up to the decimeter size) and lava lithics are included in the mass. At the base of welded facies, in the thickest sections examined, a horizon of a Plinian fall deposit constituted by pumices and ashes has been detected (Fig. 2b). The CIV appears more porous and less dense compared to the ICV, and the vertical discontinuities crossing the welded facies are more sparse.

The ignimbrites were sampled for laboratory analysis in four quarries (Fig. 1b) with subvertical fronts up to some tens of meters high. Representative samples of the welded facies were obtained from block cut in the fresh quarry fronts. On-site tests included pumping tests on wells intersecting the two types of pyroclastic flow deposits.

Field and laboratory methods

Outcrop surveys

Outcrop surveys of the two ignimbrites were carried out using the areal sampling method (Wu and Pollard 1995). Relevant outcrops (9 outcrops of the ICV and 11 outcrops of the CIV, Fig. 1b) were selected ensuring that the sampling sections included perpendicularly orientated planes for each ignimbrite. On sampling surfaces 8 to 40 m long and 3 to 30 m high, fracture data were collected and mapped through analysis of photographs. Fracture orientation (strike, dip, and dip direction), length, and spacing (perpendicular to nearest fracture of the same orientation) of each fracture that intersects the sampling plane were measured. Measurements of aperture and roughness profile (the Joint Roughness Coefficient; Barton and Choubey 1977) were carried out on un-weathered fractures, on site and by analysis of photographic images. The data collected from the different

Fig. 2 Examples of ICV (**a**) and CIV (**b**) survey outcrops (a horizon of pumices and ashes is visible at the base of the welded facies of the CIV)

outcrops were processed together to characterize the fracturing of each ignimbrite.

Laboratory tests

Hydraulic conductivity measurements

Hydraulic conductivity measurements were obtained by testing 10 rock samples in the laboratory: 6 rock samples of ICV and 4 of CIV. In the laboratory, irregular samples of the two ignimbrites (Fig. 3) were shaped and polished using a coring machine (MATEST, Italy, A140-01 model), an electric saw (Husqvarna, Italy, TS 230 F model), and a polisher machine (Buehler, Germany, AutoMet Grinder-Polishers model) to obtain 54.74 mm diameter and 102 mm height cylindrical specimens (Fig. 3). The cylindrical rock specimens were prepared according to the standard ASTM D 4525–90 (2001). A digital vernier caliper was used to check the diameter and height of the specimens.

Hydraulic conductivity measurements were performed on saturated rock samples, after immersing the specimens in distilled water for 7 days. For each ICV and CIV rock sample, 14 hydraulic tests (a total of 84 repeated measurements) and 17 hydraulic tests (a total of 68 repeated measurements) were performed, respectively.

Hydraulic conductivity tests were carried out according to the ASTM standards (ASTM D2434-68 2000 and ASTM D5084-16a 2016), by a triaxial apparatus with Hoek cell (MATEST, Italy, A137 model) equipped with permeability end caps and attachments for inflow-outflow water (MATEST, Italy,

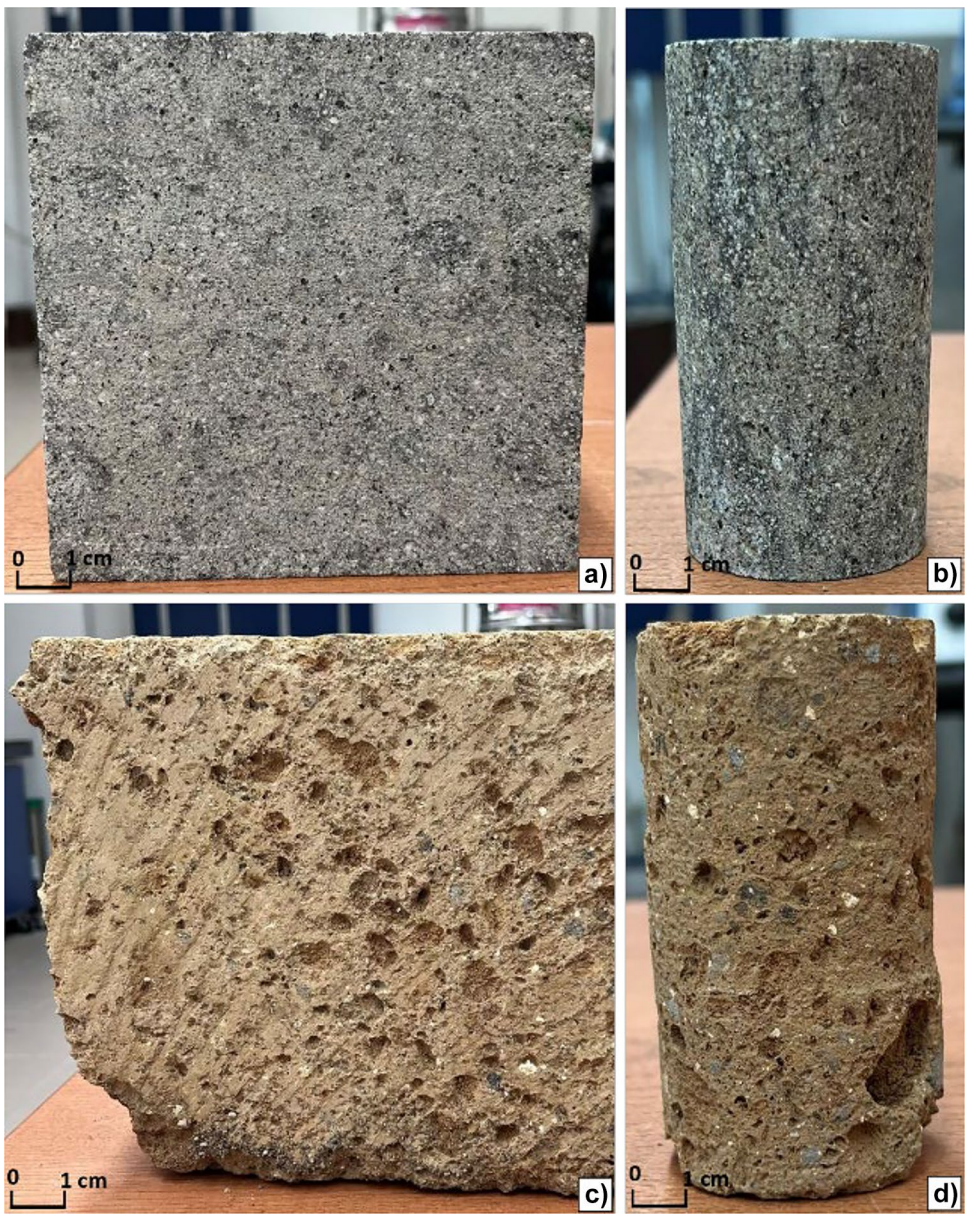

Fig. 3 Sample (**a**) and specimen (**b**) of the ICV tested, sample (**c**) and specimen (**d**) of the CIV tested

A139-05 model) (Fig. 4a). Saturated rock samples, not laterally sealed, were placed in a nitrile rubber sleeve within the Hoek cell, and then confining and water back pressures were applied and controlled. Spherical confining pressure was set by a fully automatic and high stability pressure controller system, using a compression testing machine motorized with Servo-Plus evolution control unit (MATEST, Italy, C089-19 N model). Water back pressure was regulated and controlled by a constant oil–water pressure system (MATEST, Italy, A144 model) connected with the Hoek cell (Fig. 4a). Each test, lasting up to 72 min, included 9 measurements of hydraulic conductivity.

Hydraulic conductivity, k (m/sec), was determined according to Darcy's law when the steady-state flow was reached:

$$k = \frac{q}{A \times i}$$

where q is the volumetric flow-rate of water (m^3/s), A is the cross-sectional area of the sample (m^2), and i is the dimensionless hydraulic gradient obtained by following formula:

$$i = \frac{BP}{L}$$

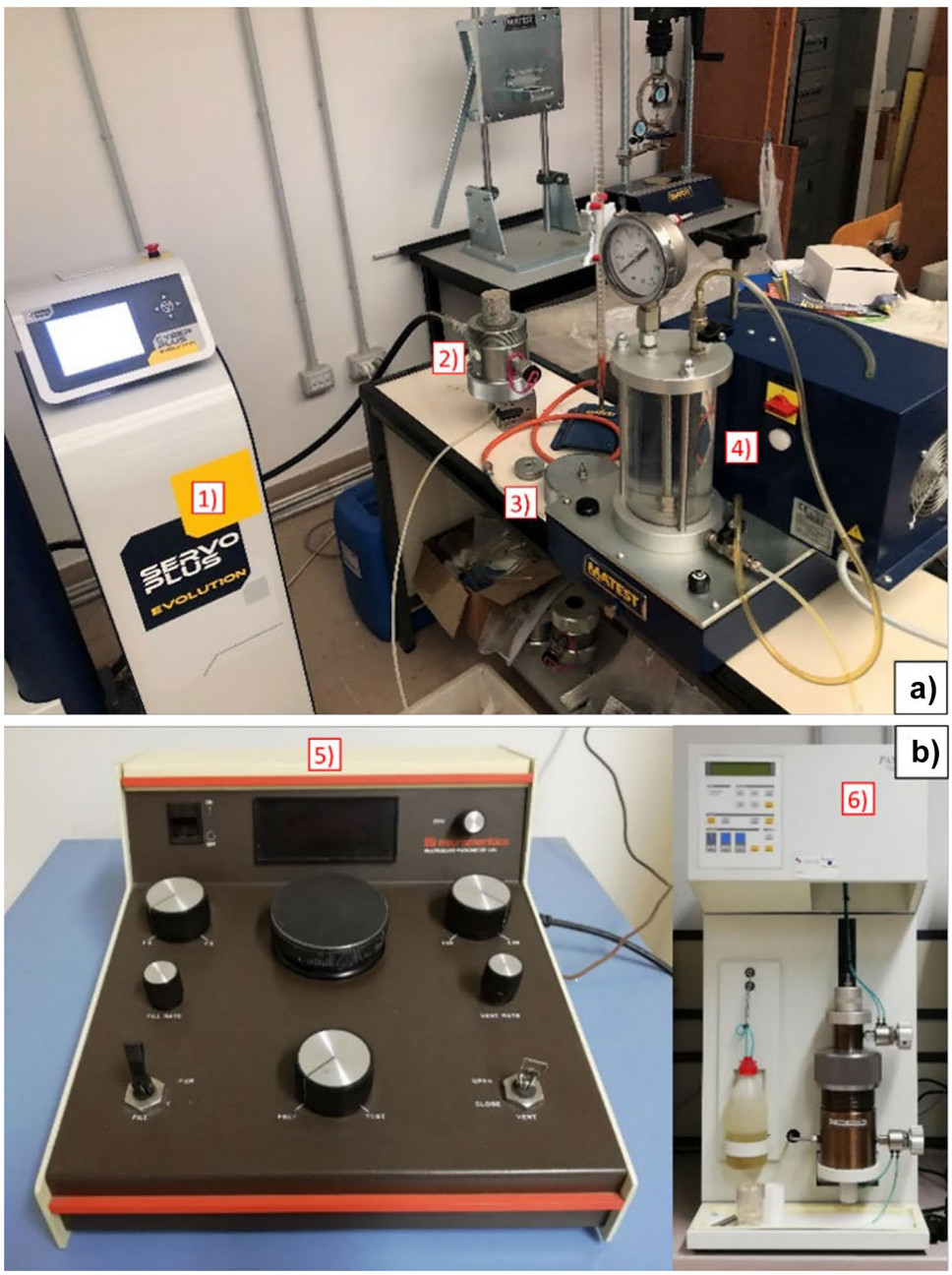

Fig. 4 Laboratory equipment for measurements of hydraulic conductivity (**a**) and porosity (**b**). 1) Servo-Plus evolution control unit of the spherical confining pressure; 2) Hoek cell with the specimen; 3) End cap; 4) Oil–water control system of the water back pressure by manometer; 5) MultiVolume Pycnometer 1305; 6) Thermo Finnigan Pascal porosimeter 140

where *BP* (MPa, converted in m of water column) is the back water pressure applied and *L* is the length of the rock sample (m). Table 1 reports the confining and water back pressures used for all the tested ICV and CIV samples. Values of confining and water back pressures were selected to test the variation of the hydraulic conductivity with depth, taking into account the thickness and the measured dry bulk density of the two ignimbrites previously determined (22.52 kN/m^3 for ICV and 14.90 kN/m^3 for CIV).

Porosity measurements

The characterization of the porous network of ignimbrites was carried out through a couple of different experimental techniques: helium pycnometry and mercury porosimetry.

Gas pycnometry is a non-destructive technique based on gas displacement using the volume-pressure relationship of Boyle's law. As an inert gas, helium is ideal for temperatures and pressures usually employed in the test and, due to its small atomic diameter, can penetrate even the smallest porous space of a material.

The MultiVolume Pycnometer 1305 gas pycnometer (99.995% pure helium, ± 0.1 to 0.2% accuracy) (Fig. 4b) was employed to measure the skeletal volume of the samples by measuring the pressure change of helium in a sample cell volume connected to a reference cell volume (at constant temperature of 24 °C and applied pressures up to 160 kPa) (ASTM D5550-14 2014). For this purpose, cylindrical specimens (26 mm diameter, lower or equal to 30 mm high) were drilled and subsequently dried in an oven at 60 °C until constant weight was achieved. The open porosity *n* (%) was then determined as the difference between bulk volume (geometric cylindrical shape measured by means of a caliper) and skeletal volume (using He pycnometer):

$$n = \left(\frac{V_b - V_g}{V_b}\right) \times 100$$

where V_b is the bulk volume and V_g is the skeletal volume.

Mercury intrusion porosimetry (MIP) is a pore size measurement technique that takes advantage of the non-wetting property of mercury to measure the size and volume distribution of pores in a wide range of porous solids, namely the range of macro-mesopore (IUPC terminology) (Rouquerol et al. 1994). Mercury is intruded into the porous structure with increasing pressure and the pore measurements (information about connected porosity, density, pore volume, pore size distribution, surface area) following the guidelines provided by ASTM D4404-18 (2018) and ISO 15901–1-2005 (2005) are based on the Washburn equation:

$$D = \frac{-4\gamma\ cos\ \theta}{P}$$

where *D* is the pore diameter (cylindrical pore shape is assumed), γ is the surface tension of mercury, θ is the contact angle of mercury, and *P* is the differential gas pressure.

For the MIP measurements, a Thermo Finnigan Pascal series porosimeter (140, 440) (Fig. 4b) was employed at a maximum pressure of 400 MPa. It was able to investigate pore diameter between 116 micron and 0.0036 micron (assuming constant values of mercury-solid contact angle equal to 140° and also of mercury surface tension ≈0.48 N/m, during test).

Pumping tests

Eighty-five pumping tests were carried out on domestic, irrigation, and drinking water wells: 40 wells intersect the ICV, and 45 wells are drilled into the CIV. The main characteristics of the tested wells are shown in Table 2.

Table 1 Confining (*CP*) and water back pressures (*BP*) used for all the tested ICV and CIV rock samples

Ignimbrite	No. test	Confining pressure (MPa)	Equivalent depth of the formation (m)	Back water pressure (MPa)
ICV	1	0.23	10	0.06; 0.12; 0.18
ICV	2	0.46	20	0.06; 0.12; 0.18; 0.25; 0.30
ICV	3	0.69	30	0.50
ICV	4	0.92	40	0.50
ICV	5	1.15	50	0.50
ICV	6	1.38	60	0.50
ICV	7	1.61	70	0.50
ICV	8	1.84	80	0.50
CIV	1	0.30	20	0.06; 0.12
CIV	2	0.45	30	0.06; 0.12; 0.18; 0.25
CIV	3	0.60	40	0.06; 0.12; 0.18; 0.25; 0.30
CIV	4	0.75	50	0.06; 0.12; 0.18; 0.25; 0.30; 0.50

Table 2 Main characteristics of the tested wells

Characteristics	Min	Max	Mean	SD	Median
Well depth (m)	25	193	77.6	34.9	72
Thickness of saturated aquifer (m)	2	95	22.4	15.6	20
Pumping flow rate (L/s)	0.2	23	3.4	4.0	2.0

The pumping tests were carried out as single-well tests; additionally, for 3 tests, observations on piezometer located close (< 30 m) to pumping well were available. All tests were carried out at a constant flow rate, and the pumping duration was between 120 and 420 min. For 10 tests, the residual drawdown during recovery was also measured.

Drawdown trend during the pumping time highlighted a condition of unsteady-state flow for most of the tests. Transmissivity values were estimated applying the Cooper and Jacob straight-line method to drawdown and recovery data (Cooper and Jacob 1946). The early-time section of drawdown in the semilog-plot was ignored to eliminate well storage effects. For the three tests carried out measuring the drawdown also in an observation well, the transmissivity values were determined by means of drawdown measured in the pumping well and in the observation well by the Cooper and Jacob method. Storativity was also estimated through drawdown data measured in the observation well.

The characterization of intersected aquifer formation of the tested wells was obtained from the stratigraphy, saturated thickness, and screen depth of the wells, when available. When direct stratigraphic information of the wells was not available, stratigraphic correlations with the surface geology and with the stratigraphy of the nearest wells were considered.

Results

Fracturing degree of the ignimbrites

Survey windows showed a number of discontinuities per m^2 between 0.025 and 0.40 (mean value 0.18, standard deviation 0.16) for the ICV and between 0.025 and 0.11 (mean value 0.076, standard deviation 0.050) for the CIV. Fractures are generally straight, with some instances of curved or wavy fractures. The fracture-orientation data collected from all outcrops of each ignimbrite are represented on the equal-area Schmidt nets of Fig. 5. Most fractures of both ignimbrites tend to be nearly vertical and are approximately N-S and E-W oriented, and the ICV is also characterized by sub-horizontal fractures (Fig. 5).

From density distribution of fracture poles, considering the discontinuities with trace length crossing the entire survey windows (i.e., those which are continuous and interconnected to the outcrop scale), three and two sets have been identified for the ICV and CIV, respectively (Table 3). The orientation of the median plane of the various sets of each ignimbrite was determined considering the point of maximum concentration of the poles on the Schmidt diagrams. For the distinguished discontinuity sets, the mean value of spacing was determined based on the discontinuity traces on the sampling windows (Table 3).

Fractures show variable apertures from a few millimeters to some centimeters. In vertical fractures, in the first meters

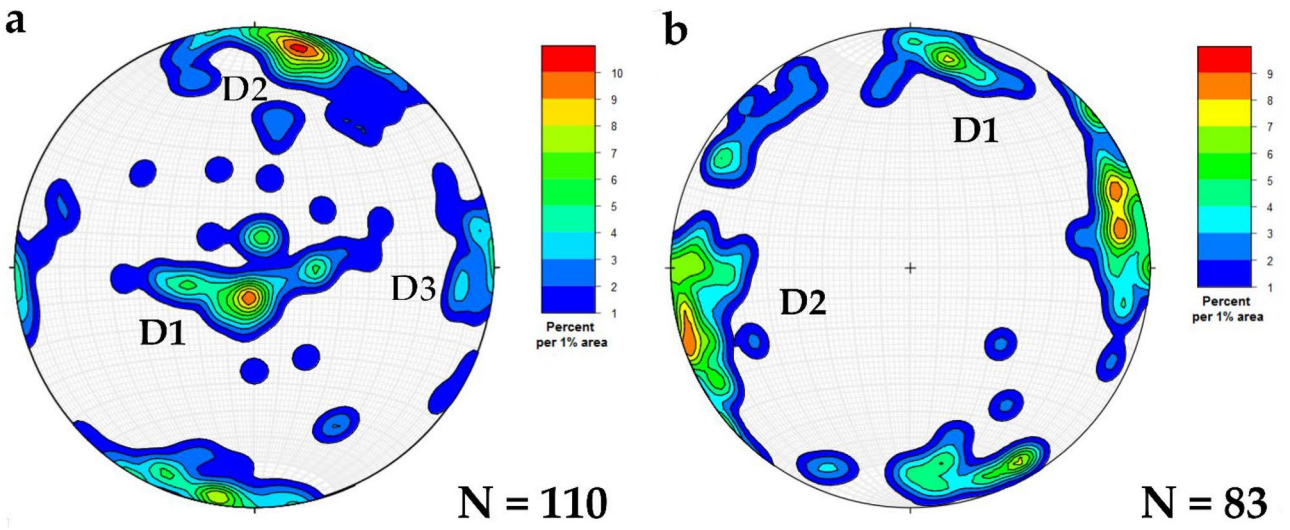

Fig. 5 Contour plots of fracture orientation projected on a lower hemisphere equal-area pole stereonet: **a** ICV and **b** CIV (N: number of measurements)

Table 3 Mean values of the strike, dip, and spacing of the persistent discontinuity sets of the two ignimbrites

Ignimbrite	Set	Strike/dip (°/°)	Spacing (m)
ICV	D1	298/10	10.5 ± 2.5
ICV	D2	102/82	3.9 ± 2.1
ICV	D3	178/85	4.8 ± 3.5
CIV	D1	98/80	6.5 ± 4.2
CIV	D2	330/86	6.3 ± 5.4

of depth, illuvial filling material derived from weathering of the ignimbrite soils has been detected. On the deepest part of the outcrops with heights greater than 10 m, the aperture was measured for un-weathered fracture traces of about 1 m long of the distinguished discontinuity sets of each ignimbrite. The statistics of the aperture measurements are summarized in Table 4, grouped for the two ignimbrites.

Based on the arithmetic mean (a_m) and standard deviation of aperture (σ), the potential hydraulic aperture (a_h') was estimated using the empirical expression of Renshaw (1995):

$$a_h' = a_m\left(1+\frac{\sigma^2}{a_m^2}\right)^{-\frac{1}{2}}$$

and that (a_h'') of Barton et al. (1985), considering the most frequent Joint Roughness Coefficient of fractures (*JRC*):

$$a_h'' = \frac{a_m^2}{JRC^{2.5}}$$

As shown in Table 5, the hydraulic aperture resulting from the two methods ranges between two orders of magnitude for the ICV and three orders of magnitude for the CIV.

Assuming the validity of the cubic law (Snow 1969; Witherspoon et al. 1980), the module of hydraulic conductivity of each fracture set was determined, considering the average spacing of each set and the estimated hydraulic apertures (assumed constant for the different sets of the same ignimbrite). Then, the matrix tensor of hydraulic conductivity of the fracture sets of each ignimbrite was calculated, considering the average set orientations. Module and orientation of principal components of the hydraulic conductivity of rock mass were finally found by eigenvalues and eigenvectors of the symmetric square matrix. In Table 6, module and orientation of the principal components of hydraulic conductivity (*K1*, *K2*, *K3*) of each ignimbrite are reported for the two estimated hydraulic apertures, as well as the geometric mean of the three principal components (*Km*) representing the composite hydraulic conductivity value of each ignimbrite.

Table 4 Statistics of aperture measurements (mm)

Ignimbrite	ICV	CIV
Number of measurements	197	179
Minimum value	0.89	0.80
Maximum value	14.81	10.00
Arithmetic mean	3.35	3.22
Standard error	0.14	0.13
Variance	4.09	3.19
Standard deviation	2.02	1.79
Median	2.96	2.80
Geometric mean	2.87	2.75
Coefficient of variation	60.36	55.53

Table 5 Fracture aperture: a_m arithmetic mean of the measured aperture, σ standard deviation, most frequent *JRC*, a_h' hydraulic aperture estimated by the Renshaw (1995) method, a_h'' hydraulic aperture estimated by the Barton et al. (1985) method

Ignimbrite	a_m (mm)	σ (mm)	*JRC*	a_h' (mm)	a_h'' (mm)
ICV	3.35	2.02	4	2.87	0.35
CIV	3.22	1.79	8	2.81	0.06

The results of this characterization of ignimbrites, based solely on secondary rock porosity, show a significant anisotropy of hydraulic conductivity of the rock mass in the vertical plane (*K1* ≠ *K2*≈*K3* in Table 6). The geometric mean of the hydraulic conductivity of the two ignimbrites is strongly influenced by the values of the hydraulic aperture, which is greatly reduced in the CIV if the higher *JRC* is taken into account (*Km* under two hypotheses of hydraulic aperture in Table 6).

Laboratory tests

Hydraulic conductivity

Table 7 summarizes the statistics of the laboratory measurement of hydraulic conductivity, distinguishing between the tests carried out on the ICV and CIV samples.

As showed in the box-and-whisker diagram (Fig. 6a), hydraulic conductivity values span over 4 orders of magnitude for the ICV and 2 orders of magnitude for the CIV. The ICV is characterized by lower values of the parameter than the CIV, whether the range of the most frequent values is taken into account (3.08×10^{-8} – 2.99×10^{-7} m/s for the ICV and 4.49×10^{-7} – 1.27×10^{-6} m/s for the CIV) or the average values are taken into consideration (median 1.09×10^{-7} m/s for the ICV and 7.68×10^{-7} m/s for the CIV).

Permeability tests conducted by varying the confining pressure of the specimens allowed to determine relationships between k and equivalent depth. As shown in Fig. 7, a decrease in hydraulic conductivity with the increasing of equivalent depth for both ignimbrites results.

Table 6 Values (m/s) and orientation (°) of principal components (*K1*, *K2*, *K3*) and geometric mean (*Km*) of hydraulic conductivity of rock mass under two hypotheses of hydraulic aperture (a_h' and a_h'', in mm)

Ignimbrite	ICV, a_h' = 2.87	ICV, a_h'' = 0.35	CIV, a_h' = 2.81	CIV, a_h'' = 0.06
K1				
Value	1.87×10^{-3}	0.34×10^{-5}	0.07×10^{-3}	0.07×10^{-8}
Trend/plunge	38/86	38/86	344/86	344/86
K2				
Value	8.98×10^{-3}	1.63×10^{-5}	5.60×10^{-3}	5.45×10^{-8}
Trend/plunge	207/4	207/4	202/3	202/3
K3				
Value	10.79×10^{-3}	1.96×10^{-5}	5.67×10^{-3}	5.52×10^{-8}
Trend/Plunge	297/1	297/1	112/2	112/2
Km	5.66×10^{-3}	1.03×10^{-5}	1.30×10^{-3}	1.28×10^{-8}

Porosity

Table 8 summarizes the statistics of the laboratory measurement of porosity obtained by He-pycnometry, distinguishing between the tests carried out on the ICV and CIV samples.

The ICV has a significantly lower porosity than the CIV, both in terms of average (median value of 19 and 50.5% for ICV and CIV, respectively) and most frequent values (from 14 to 20% for the ICV and from 48 to 51% for the CIV) (Fig. 6b). In particular, the CIV can be classified as highly porous materials, strongly depending on the high pumice content of this ignimbrite.

Through MIP a more detailed investigation of the pore volume for the CIV and ICV has been obtained. The main results of the MIP analysis are given in Table 9.

The average MIP porosity values are lower than those found through the He pycnometry. This is due to the possibility of the helium gas to rapidly penetrate even in small pores, while the MIP technique is unable to measure micropores (diameter < 0.002 micron). Again, however, the porosity of the CIV is significantly higher than that of the ICV, as well as the specific surface area equal to 10.65 m^2/g for the CIV and 2.50 m^2/g for the CIV (Table 9). Little difference between the two ignimbrites results in terms of average pore size (about 0.1 μm) and median pore diameter volume (4.15 and 3.84 μm for the ICV and CIV, respectively). The detail about the pore size is shown in the frequency distribution of Fig. 8. The graphs of the two ignimbrites essentially indicate unimodal spectrums with frequency peaks well within the macropore range. In particular, the CIV pattern uniformly decreases towards mesopores, while ICV pattern exhibits a tendency to an unequal unimodal structure.

Table 7 Statistics of the laboratory measurement of hydraulic conductivity (m/s) on rock samples

Ignimbrite	ICV	CIV
Number of tests	84	68
Number of measurement	756	612
Minimum value	1.23×10^{-9}	1.14×10^{-7}
Maximum value	3.06×10^{-6}	5.92×10^{-6}
Arithmetic mean	3.64×10^{-7}	1.10×10^{-6}
Standard error	2.08×10^{-8}	4.55×10^{-8}
Variance	3.24×10^{-13}	1.14×10^{-12}
Standard deviation	5.69×10^{-7}	1.07×10^{-7}
Median	1.09×10^{-7}	7.68×10^{-7}
Geometric mean	1.01×10^{-7}	7.62×10^{-7}
Coefficient of variation	156.56	96.84

Pumping tests

The wells tested in the ICV intersect the welded and fractured facies of the ignimbrite, reaching the low-permeability sedimentary substrate. In some cases, at the base of the welded and fractured layer, an agglomerate formed by blocks of ignimbrite and lava dome is present. The wells tested in the CIV intersect massive and welded facies of the ignimbrite and frequently its base, including layers of pumices and breccia.

Most of the drawdown-time relationships detected during pumping and recovery show a good adaptation to the Cooper-Jacob model, highlighting the behavior of the aquifer as confined aquifer or leaky aquifer. This is consistent with observations during well drilling, that is, the rise of the water level in the borehole after intercepting the aquifer formation.

For the tests regarding recovery measurement, the complete recovery of the initial water level was achieved in intervals no longer than the pumping time. The transmissivity values obtained from the 10 recovery test (T_r) were compared with those estimated through the drawdown measured during the pumping (T_d). T_r and T_d are in agreement with the following relationship ($R^2 = 0.99$):

$$T_r = 0.3622\ T_d^{0.8961} \quad (1)$$

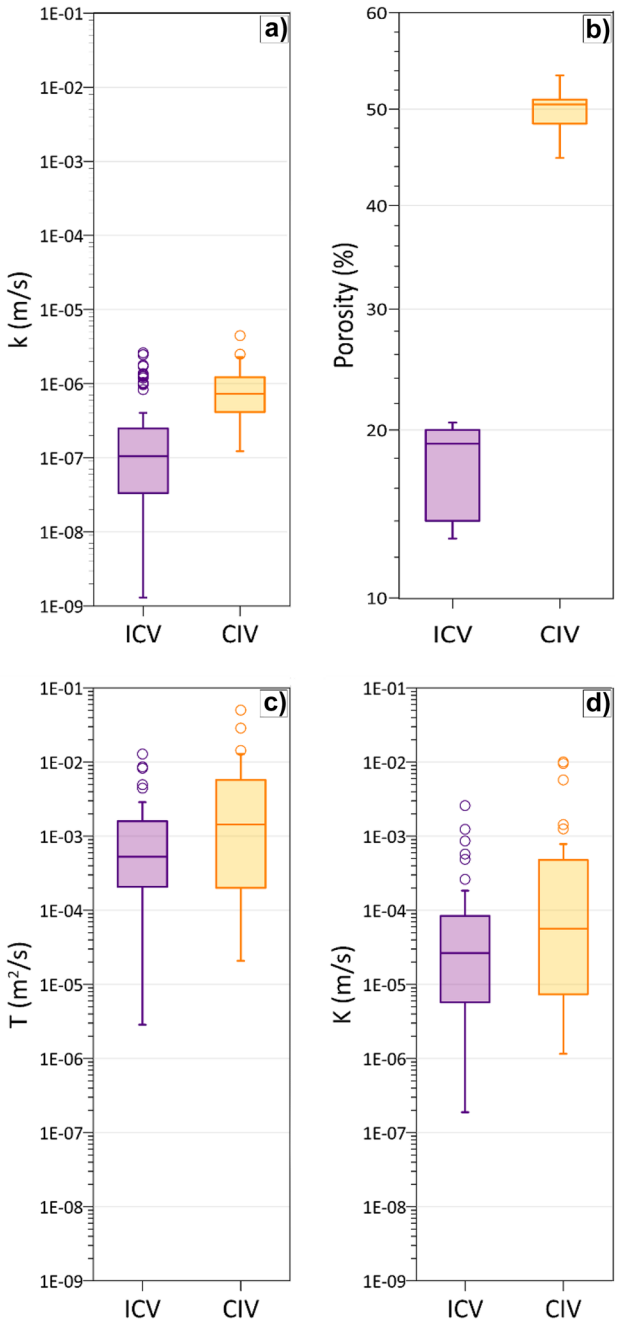

Fig. 6 Box-and-whisker diagrams for ICV and CIV: **a** laboratory measurement of hydraulic conductivity, **b** porosity values obtained by He-pycnometry, **c** transmissivity, and **d** hydraulic conductivity values obtained from pumping tests

From Eq. (1), T_r was determined for all other texts for which only T_d was available. The values thus determined have been assumed as the transmissivity of the aquifer (T), being the residual drawdown less influenced by well losses.

The statistics of the transmissivity data obtained are summarized in Table 10, distinguishing between the tests carried out on the ICV and the CIV.

Transmissivity values span over 5 orders of magnitude and 4 orders of magnitude for the ICV and the CIV, respectively (Fig. 6c). Although the most frequent values fall in the order of magnitude 10^{-4}–10^{-3} m^2/s for both formations, the ICV is characterized by a lower average value (geometric mean 4.35×10^{-4} m^2/s) than the CIV (geometric mean 1.12×10^{-3} m^2/s).

By relating the transmissivity value (T) to the saturated aquifer thickness (b), the hydraulic conductivity has been obtained ($K = T/b$).The statistics of the hydraulic conductivity data obtained for each formation are summarized in Table 11.

Hydraulic conductivity values span over 4 orders of magnitude for the ICV and the CIV (Fig. 6d). The most frequent values fall in the order of magnitude $10^{-6} – 10^{-5}$ m/s for the ICV and $10^{-6} – 10^{-4}$ m/s for the CIV. A lower average value characterizes the ICV (geometric mean 2.08×10^{-5} m/s) compared with the CIV (geometric mean 7.49×10^{-5} m/s).

For the three pumping tests performed with measurements in the piezometer, transmissivity estimated by recovery data measured in the pumping well little differs from that obtained through the data measured in the piezometer. The storativity (S) between 1.40×10^{-3} and 4.96×10^{-3} for the ICV and 1.31×10^{-3} for the CIV result from this type of testing. These storativity values were then compared with porosity (n) according to the following relationship:

$$S = b\left[\rho g(\alpha + \beta n)\right] \tag{2}$$

where b is aquifer thickness, ρ is mass density of water, g is gravitational acceleration, α is aquifer compressibility, and β compressibility of water.

Discussion

The multiscale investigations allowed to examine the role of the matrix and fractures on the hydrological behavior of the two ignimbrites different in age, composition, and origin.

Matrix permeability obtained from laboratory tests is higher for the CIV than for the ICV; this applies both to the average value (median of 7.68×10^{-7} and 1.09×10^{-7} m/s, respectively for CIV and ICV) and to the most frequent values of hydraulic conductivity (4.49×10^{-7}– 1.27×10^{-6} m/s for CIV and 3.08×10^{-8}– 2.99×10^{-7} m/s for ICV). This seems to be consistent with the higher degree of welding of the ICV than the CIV. In fact, in accordance with the literature, the more densely welded ignimbrites are lower in matrix permeability and primary porosity (Fuller and Sharp 1992; Sharp et al. 1993; Smyth and Sharp 2006).

Moreover, the matrix porosity determined on the rock samples shows higher values for the CIV than for the ICV through both He-pycnometry (median values of 50 and 19%

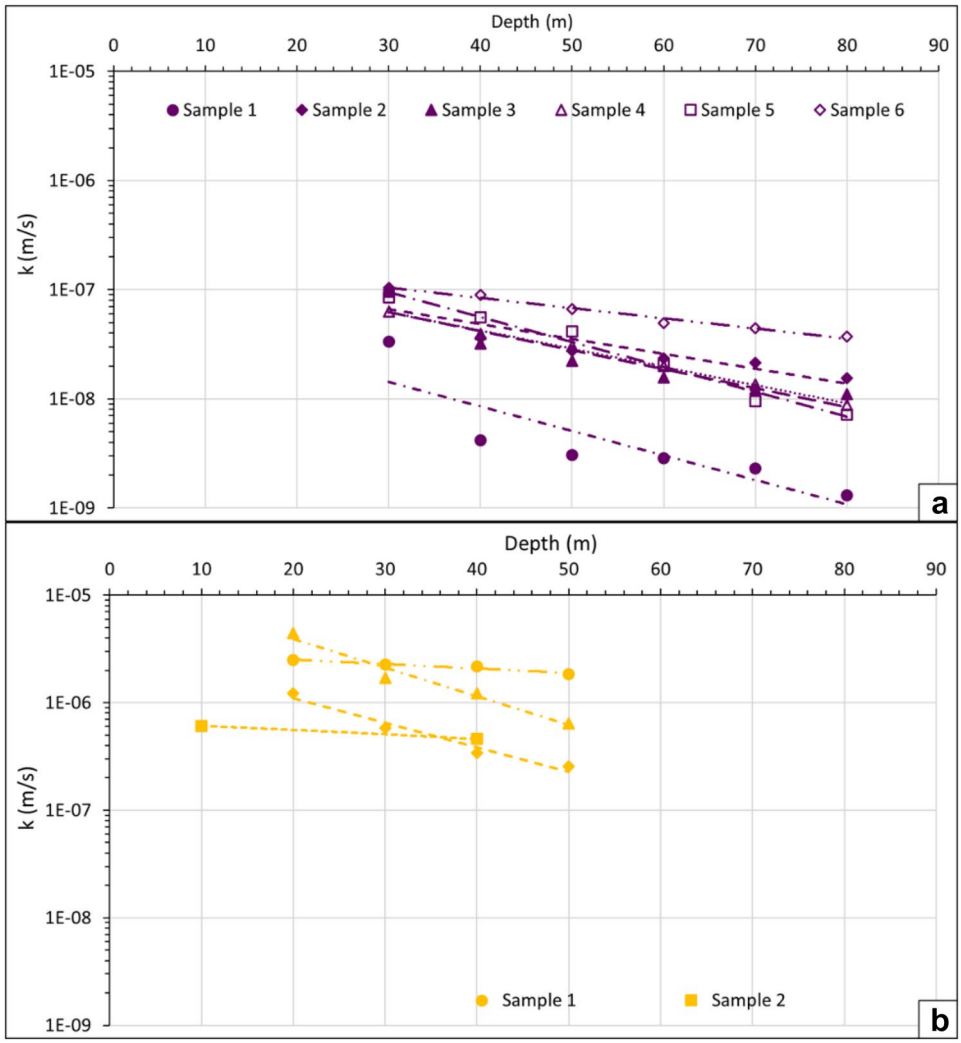

Fig. 7 Relationships between hydraulic conductivity (*k*) and equivalent depth for ICV (**a**) and CIV (**b**)

for CIV and ICV, respectively) and MIP techniques (average values of 41 and 14% for CIV and ICV, respectively). The two ignimbrites also differ for the specific surface area measured by the MIP, higher for the CIV (10.65 m^2/g) than for the ICV (2.50 m^2/g). The contrast in the porosity values between the two ignimbrites can be related to the difference in welding degree, depositional processes occurring during cooling, and in the post-cooling stages, which affect primary textural and structural features (Sruoga et al. 2004; Koralay et al. 2011; Colella et al. 2017). Specifically, the higher porosity of CIV is due to the greater pumice content and presence of large pumices cavities, in addition to its lower degree of welding if compared with the ICV.

Table 8 Statistics of porosity values (He-pycnometry, %) of rock samples

Ignimbrite	ICV	CIV
Number of tests	11	21
Number of measurement	55	105
Minimum value	13.01	44.9
Maximum value	20.54	53.53
Arithmetic mean	17.37	49.91
Standard error	0.92	0.49
Variance	9.29	5.13
Standard deviation	3.05	2.26
Median	19	50.5
Geometric mean	17.12	49.86
Coefficient of variation	17.54	4.54

Table 9 Porosity data of ignimbrites measured by mercury intrusion porosimetry (MIP). The values are an average of six samples (standard deviations are reported in brackets)

Ignimbrite	ICV	CIV
MIP porosity (%)	14.51 (± 3.10)	40.62 (± 2.08)
Specific surface area (m^2/g)	2.50 (± 1.13)	10.65 (± 1.45)
Average pore diameter (μm)	0.116 (± 0.033)	0.117 (± 0.013)
Median pore diameter (μm)	4.15 (± 0.90)	3.84 (± 0.63)

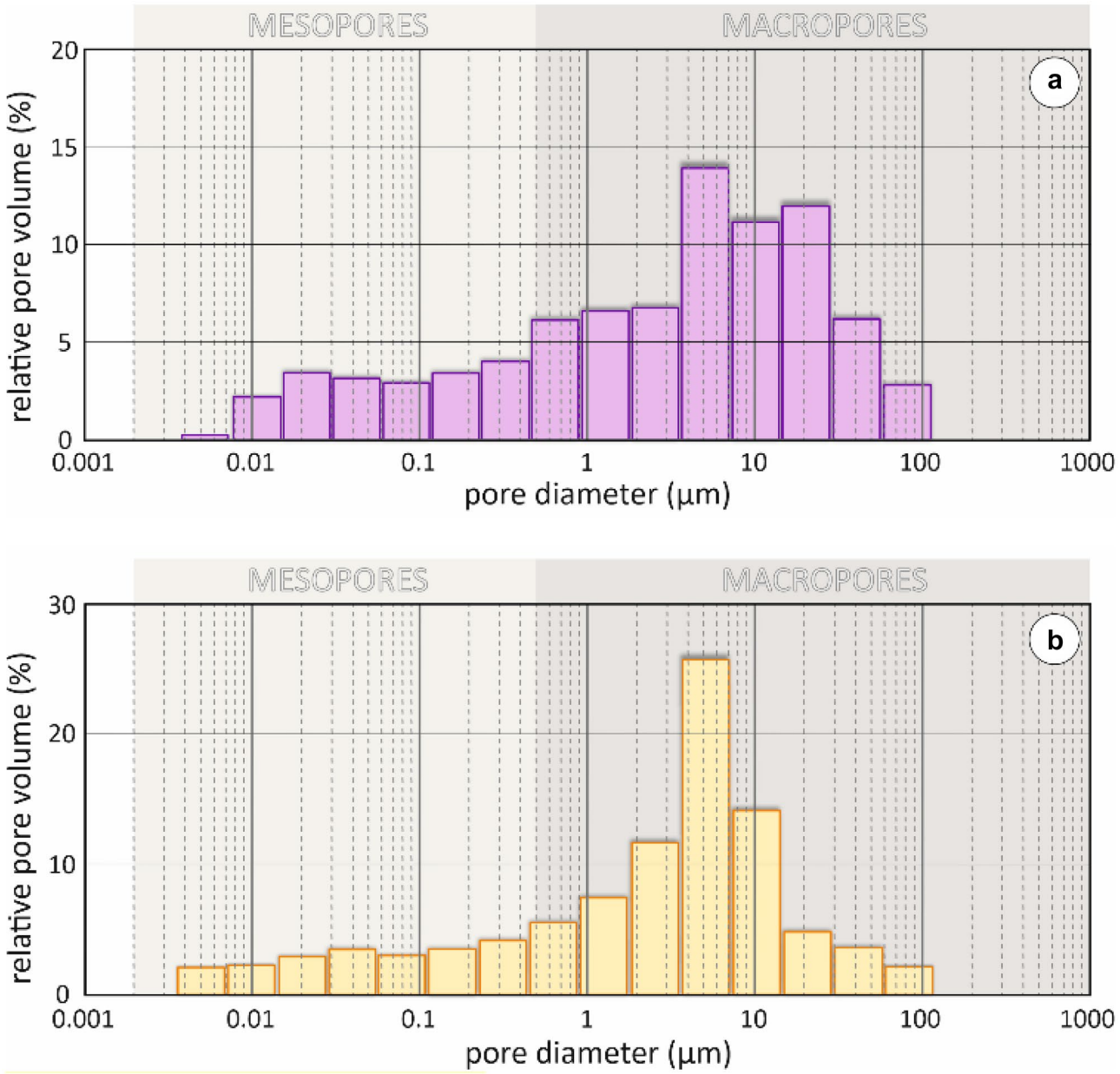

Fig. 8 Pore-size distribution for ICV (**a**) and CIV (**b**)

With regard to the degree of welding of the two ignimbrites, a specific assessment can be obtained considering the known physical properties of the two deposits, i.e., bulk density (22.52 kN/m^3 for ICV and 14.90 kN/m^3 for CIV) and porosity (14–19% for ICV and 41–50% for CIV) determined in this study, and uniaxial compressive strength reported in the literature (21.4–22.0 MPa for ICV and 3.5–6.0 MPa for CIV; Ottaviani 1988). Based on these physical properties, as well as on the textural and structural features observed in the field, the ICV and CIV are placed, respectively, in Rank IV and II, according to welding ranking of Quane and Russell (2005).

By comparing porosity and permeability of the matrix, the greater difference is found between the two ignimbrites in terms of matrix porosity rather than that resulting for matrix hydraulic conductivity. Probably, the higher specific surface area of the CIV tends to retain more water in the pores, thus reducing the effective porosity. As it is widely reported in the literature, the matrix permeability of these pyroclastic rocks is related to effective porosity rather than total porosity (e.g., Flint and Selker 2003). This is in accordance with the Kozeny-Carman equation (Carman 1956) which relates permeability, in addition to porosity, to the inverse of the square of the specific surface area.

Table 10 Statistics of transmissivity values (m^2/s)

Ignimbrite	ICV	CIV
Number of tests	40	45
Minimum value	2.86×10^{-6}	2.08×10^{-5}
Maximum value	1.29×10^{-2}	5.03×10^{-2}
Arithmetic mean	1.65×10^{-3}	5.52×10^{-3}
Standard error	4.32×10^{-4}	1.43×10^{-3}
Variance	7.47×10^{-6}	9.28×10^{-5}
Standard deviation	2.73×10^{-3}	9.63×10^{-3}
Median	5.32×10^{-4}	1.44×10^{-3}
Geometric mean	4.35×10^{-4}	1.12×10^{-3}
Coefficient of variation	165.64	174.40

The contribution of matrix permeability to the permeability of the entire ignimbrite unit can be deduced from the results of the pumping tests. These tests show values for hydraulic conductivity of two orders of magnitude greater than that of the matrix (geometric mean from 2.08×10^{-5} to 7.49×10^{-5} and m/s for the two ignimbrites). The highest hydraulic conductivity found through pumping tests can be attributed to the largest volume of aquifer concerning this type of test and thus to the prevailing contribution of fractures on rock mass permeability, according to previous studies (e.g., Smyth and Sharp 2006).

To analyze the influence of fracture permeability on the rock mass, the results of fracturing degree characterization are to be considered. Both the fracture density and the hydraulic conductivity determined by cubic law applied to persistent discontinuities turn out to be higher for ICV than CIV. With regard to the determination of hydraulic conductivity, it should be noted that the values obtained for the two ignimbrites (geometric mean *Km*) are to be understood in relative terms and characterizing the fracture frequency and number of the discontinuity sets of the two rock formations. This is a consequence of the simplifications adopted in the calculation for hydraulic aperture, assumed constant for the different sets and derived from empirical relationships with measured mechanical aperture. Therefore, by comparing in relative terms the *Km* values obtained for the two ignimbrites, according to the two hypotheses of hydraulic aperture, the ICV, the ignimbrite with the higher degree of welding, is certainly to be considered more permeable by fracture. This would be consistent with what is known in the literature, namely that fracture permeability is greater in more densely welded ash flow tuffs (Winograd 1971; Fuller and Sharp 1992; Smyth and Sharp 2006; Wohletz 2006). Hence, the difference found in fracture permeability of the two ignimbrites is mainly due to the presence of more discontinuity sets and a lower spacing for the ICV than the CIV. The ratio of *Km* between the ICV and the CIV increases from 4 to 805 depending the model used to determine the hydraulic aperture; the largest difference of *Km* in the second case is related to the roughness of the fractures, considered by the expression of Barton et al. (1985), higher for the CIV fractures.

Table 11 Statistics of hydraulic conductivity values (m/s) obtained from pumping tests

Ignimbrite	**ICV**	**CIV**
Number of tests	40	45
Minimum value	1.89×10^{-7}	1.16×10^{-6}
Maximum value	2.59×10^{-3}	1.01×10^{-2}
Arithmetic mean	1.78×10^{-4}	8.28×10^{-4}
Standard error	7.36×10^{-5}	3.23×10^{-4}
Variance	2.17×10^{-7}	4.70×10^{-6}
Standard deviation	4.65×10^{-4}	2.17×10^{-3}
Median	2.65×10^{-5}	5.67×10^{-5}
Geometric mean	2.08×10^{-5}	7.49×10^{-5}
Coefficient of variation	260.78	261.59

The hydraulic conductivity values obtained from the surveys on the outcrops are therefore influenced by the measurements at the surface of mechanical aperture. In this regard, it must be considered that a reduction in aperture with depth is certainly to be expected due to the lithostatic pressure. This can be deduced from laboratory tests, which showed a decrease in the hydraulic conductivity of the matrix as the confining pressure of the sample increased. The same effect is to be expected for the mechanical aperture of fractures.

The comparison between the hydraulic conductivity values obtained from the pumping tests for the two ignimbrites shows that the CIV is more permeable than the ICV, both on the basis of the mean values (geometric mean of 7.49×10^{-5} and 2.08×10^{-5} m/s, respectively) and on the basis of the most frequent ranges ($5 \times 10^{-6} - 8 \times 10^{-5}$ and $7 \times 10^{-6} - 5 \times 10^{-4}$ m/s, respectively). The latter finding seems to be in contrast with the analysis of fracturing degree of the two ignimbrites. The explanation of this result is to be found in the stratigraphic setting of the area examined. ICV pumping tests were conducted on wells penetrating densely welded ignimbrite facies, sometimes including its basal agglomerate layer. In the case of the CIV, wells penetrate the welded facies of the ignimbrite and frequently the basal Plinian pumice layers. Therefore, while in the case of the ICV the hydraulic conductivity derived from the pumping tests is mainly attributable to that of fractures and the matrix of welded facies, in the case of the CIV, the influence of unconsolidated pyroclastic fall deposits shall also be considered. These deposits, consisting of lapilli with scarce ash matrix, can represent a layer with high permeability and primary porosity that also allows the connection of vertical fracture sets, increasing the hydraulic conductivity on the whole (fracture-matrix of welded facies plus unconsolidated pyroclastic deposits).

Concerning the storage capacities of the two ignimbrites, the porosity values were compared with the few determination of the storativity obtained from pumping tests on the basis of Eq. (2). Considering the compressibility of the two ignimbrites (5×10^{-9} and 1×10^{-10} m^2/N for CIV and ICV, respectively) derived from the values of the Young module available in the literature (Ottaviani 1988; Bozzano et al. 2005), the compressibility of the water (4.4×10^{-10} m^2/N), the average thicknesses of the two aquifers (18 and 25 m for CIV and ICV, respectively), and the average porosity values of the matrix (0.41–0.50 and 0.14–0.19 for CIV and ICV, respectively), the storativity has been calculated. A value of 9.1×10^{-4} results for the CIV, which is consistent with that obtained from the pumping tests (1.3×10^{-3}). A value of 4.5×10^{-5} results for the ICV, which is very different from data obtained from the pumping tests ($1.4–5.0 \times 10^{-3}$). Unlike the CIV, the storage capacity of the ICV seems to be due not only to the porosity of the matrix, but also and above all to the porosity of the network of discontinuities, denser in this type of ignimbrite.

Conclusions

Investigations carried out on two ignimbrites of Central Italy, different in age, composition, and origin, have allowed to deepen the knowledge on the hydrological properties of pyroclastic flow deposits. The degree of welding, composition, and stratigraphy of the two ignimbrites are the main factors determining the hydrological properties of the pyroclastic formations examined.

The two ignimbrites share a low matrix permeability, showing a different fracturing degree. The more welded ignimbrite is characterized by lower porosity of the matrix and higher fracturing degree, while the less welded ignimbrite is characterized by higher porosity of the matrix and lower fracturing degree.

On a scale greater than 100 m^3, hydraulic conductivity and storage capacity of the highly welded ICV, characterized by a higher dry bulk density and a lower porosity, mainly depend on the denser network of discontinuities. In fact, less spaced vertical and horizontal fractures characterize this ignimbrite. The hydraulic conductivity of the younger CIV, less welded, mainly depend on the sparser network of discontinuities and on the layer of unconsolidated coarse pyroclastic deposits at its base, while the storage capacity depends on the more porous matrix.

The hydrological characterization of these pyroclastic formations, whether the objective is their use as aquifers for water supply or substratum of waste disposal sites, must necessarily include different scales of analysis. It is also necessary that the results of laboratory and on-site tests are correctly interpreted taking into account the stratigraphy of the ignimbrite, which means knowing origin, composition, and emplacement of the pyroclastic flows.

Acknowledgements The authors are grateful to Dr E. Di Clemente for the assistance during the hydraulic conductivity measurements, and Mr S. Dei and Dr F. Rossi for allowing the sampling and surveys in the quarries. The authors would like to thank the two anonymous reviewers for their constructive comments and discussions, which helped to improve the manuscript.

Author contributions V. Allocca, A. Colella and V. Piscopo contribute equally to this work: writing—original draft, conceptualization, and review and editing. V. Piscopo performed supervision. P. Colantuono and S.M. Piacentini provide laboratory and in-situ tests.

References

ASTM D2434–68 (2000) Standard test method for permeability of granular soils (Constant Head). ASTM International, West Conshohocken, PA. www.astm.org

ASTM D4404–18 (2018) Standard test method for determination of pore volume and pore volume distribution of soil and rock by mercury intrusion porosimetry. ASTM International, West Conshohocken, PA. www.astm.org

ASTM D4525–90 (2001) Standard test method for permeability of rocks by flowing air. ASTM, 100 Barr Harbor Drive, West Conshohocken, PA. www.astm.org

ASTM D5084–16a (2016) Standard test methods for measurement of hydraulic conductivity of saturated porous materials using a flexible wall permeameter. ASTM International, West Conshohocken, PA. www.astm.org

ASTM D5550–14 (2014) Standard test method for specific gravity of soil solids by gas pycnometer. ASTM International, West Conshohocken, PA. www.astm.org

Barton N, Bandis SC, Bakhtar K (1985) Strength, deformation and conductivity coupling of rock joints. Int J Rock Mech Min Sci Geomech Abstr 22:121–140

Barton N, Choubey V (1977) The shear strength of rock joints in theory and practice. Rock Mech 10:1–54

Bertagnini A, Sbrana A (1986) Il vulcano di Vico: stratigrafia del complesso vulcanico e sequenze eruttive delle formazioni piroclastiche. Mem Soc Geol It 35:699–713

Bozzano F, Floris M, Gaeta M, Martino S, Scrarascia Mugnozza G (2005) Geological setting and gravity-induced evolution of volcanic cliffs in northern Latium (Italy). Boll Soc Geol It 124:413–436

Carlino S, Piochi M, Tramelli A, Mormone A, Montanaro C, Scheu B, Mayer K (2018) Field-scale permeability and temperature of

volcanic crust from borehole data: Campi Flegrei, southern Italy. J Volcanol Geotherm Res 357:276–286
Carman PC (1956) Flow of gases through porous media. Academic Press Inc, New York
Cimarelli C, De Rita D (2006) Structural evolution of the Pleistocene Cimini trachytic volcanic complex (Central Italy). Bull Volcanol 68:538–548
Colella A, Di Benedetto C, Calcaterra D, Cappelletti P, D'Amore M, Di Martire D, Graziano SF, Papa L, Langella A (2017) The Neapolitan Yellow Tuff: an outstanding example of heterogeneity. Constr Build Mater 136:361–373
Conticelli S, Peccerillo A (1992) Petrology and geochemistry of potassic and ultrapotassic volcanism in Central Italy: petrogenesis and inferences on the evolution of the mantle source. Lithos 28:221–240
Cooper HH, Jacob CE (1946) A generalized graphical method for evaluating formation constants and summarizing well field history. Trans Am Geophys Union 27:526–534
Fisher RV, Schmincke HU (1984) Pyroclastic rocks. Springer-Verlag, Berlin
Flint LE, Selker JS (2003) Use of porosity to estimate hydraulic properties of volcanic tuff. Adv Water Res 26:561–571
Foster SD, Ellis AT, Losilla-Penon M, Rodiguez-Estrada HV (1985) Role of volcanic tuffs in ground-water regime of Valle Central, Costa Rica. Groundwater 23(6):795–801
Fuller CM, Sharp JM (1992) Permeability and fracture patterns in extrusive volcanic rocks: implications from the welded Santana Tuff, Trans-Pecos Texas. Geol Soc Amer Bull 104:1485–1496
Heap MJ, Baud P, Meredith PG, Vinciguerra S, Reuschlé T (2014) The permeability and elastic moduli of tuff from Campi Flegrei, Italy: implications for ground deformation modelling. Solid Earth 5:25–44
ISO 15901–1–2005 (2005) Pore size distribution and porosity of solid materials by mercury porosimetry and gas adsorption - Part 1: Mercury porosimetry. ISO, Geneva, Switzerland
Istok JD, Rautman CA, Flint LE, Flint AL (1994) Spatial variability in hydrologic properties of volcanic tuff. Groundwater 32(5):751–760
Koralay T, Özkul M, Kumsar H, Çelik SB, Pektaş K (2011) The effect of welding degree on geotechnical properties of an ignimbrite flow unit: the Bitlis castle case (eastern Turkey). Environ Earth Sci 64:869–881
Lahoud RG, Lobmeyer DH, Whitfield MS (1984) Geohydrology of volcanic tuff penetrated by test well UE-25b#1, Yucca Mountain, Nye County, Nevada. US Geol Survey Water Res Inv Report 84–4253
Lardini D, Nappi G (1987) I cicli eruttivi del complesso vulcanico Cimino. Rend Soc Ital Petrol 42:141–153
Locardi E (1965) Tipi di ignimbrite di magmi mediterranei. Le ignimbriti del Vulcano di Vico. Atti Soc Tosc Sc Nat 72:55–173
Nappi G, Valentini L, Mattioli M (2004) Ignimbritic deposits in Central Italy: pyroclastic products of the quaternary age and Etruscan footpaths. In: 32nd International Geological Congress, Florence, August 20–28, 2004, APAT, Rome (Field Guide Book P09)
Micheluccini M, Puxeddu M, Toro B (1971) Rilevamento e studio geo-vulcanologico della regione del M. Cimino (Viterbo-Italia). Atti Soc Tosc Sc Nat 78:301–337
Montanaro C, Scheu B, Mayer K, Orsi G, Moretti R, Isaia R, Dingwell DB (2016) Experimental investigations on the explosivity of steam-driven eruptions: a case study of Solfatara volcano (Campi Flegrei). J Geophys Res Solid Earth 121:7996–8014
Ottaviani M (1988) Proprietà geotecniche di tufi vulcanici italiani. Riv It Geotecnica 3:173–178
Peccerillo A (2005) Plio-Quaternary volcanism in Italy. Springer, Berlin
Peccerillo A, Manetti P (1985) The potassium alkaline volcanism of central-southern Italy: a review of the data relevant to petrogenesis and geodynamic significance. Trans Geol Soc Afr 88:379–384
Peluso F, Arienzo I (2007) Experimental determination of permeability of Neapolitan Yellow Tuff. J Volcanol Geotherm Res 160:125–136
Perini G, Conticelli S, Francalanci L (1997) Inferences on the volcanic history of the Vico volcano, Roman Magmatic Province, Central Italy: stratigraphic, petrographic and geochemical data. Miner Petrogr Acta 40:67–93
Peters RR, Klavetter EA (1988) A continuum model for water movement in an unsaturated fractured rock mass. Water Resour Res 24(3):416–430
Quane SL, Russell JK (2005) Ranking welding intensity in pyroclastic deposits. Bull Volcanol 67:129–143
Rasmussen TC, Evans DD, Sheets PJ, Blandford JH (1993) Permeability of the Apache Leap Tuff: borehole and core measurements using water and air. Water Resour Res 29(7):1997–2006
Renshaw CE (1995) On the relationship between mechanical and hydraulic aperture in rough-walled fractures. J Geophys Res Solid Earth 100:24629–24636
Rouquerol J, Avnir D, Fairbridge CW, Everett DH, Haynes JH, Pernicone N, Ramsay JDF, Sing KSW, Unger KK (1994) Recommendations for the characterization of porous solids. Pure Appl Chem 66(8):1739–1758
Sharp JM, Smyth-Boulton RC, Fuller CM (1993) Permeability and fracture patterns in a weathered and variably welded tuff: implications for flow and transport. In: Memories of the XXIVth Congress of IAH, As (Oslo), pp 103–114
Smyth RC, Sharp JM (2006) The hydrogeology of tuffs. In: Heiken G (ed) Tuffs – Their properties, uses, hydrology, and resources. Geol Soc Amer 408:91–111 (Special Paper)
Snow DT (1969) Anisotropic permeability of fractured media. Water Resour Res 5:1273–1289
Sollevanti F (1983) Geologic, volcanologic, and tectonic setting of the Vico-Cimino area, Italy. J Volcanol Geotherm Res 17:203–217
Sparks RSJ, Self S, Walker GPL (1973) Products of ignimbrite eruption. Geology 1:115–118
Sruoga P, Rubinstein N, Hinterwimmer G (2004) Porosity and permeability in volcanic rocks: a case study on the Serie Tobífera, South Patagonia, Argentina. J Volcanol Geotherm Res 132:31–43
Vanorio T, Prasad M, Patella D, Nur A (2002) Ultrasonic velocity measurements in volcanic rocks: correlation with microtexture. Geophys J Int 149:22–36
Winograd IJ (1971) Hydrogeology of ash flow tuffs: a preliminary statement. Water Resour Res 7:994–1006
Witherspoon PA, Wang JS, Iwai K, Gale JE (1980) Validity of cubic law for fluid flow in a deformable rock fracture. Water Resour Res 16:1016–1024
Wohletz K (2006) Fractures in welded tuff. In: Heiken G (ed) Tuffs - Their properties, uses, hydrology, and resources. Geol Soc Amer 408:17–31 (Special Paper)
Wu H, Pollard DD (1995) An experimental study of the relationship between joint spacing and layer thickness. J Struct Geol 17:887–905
Flint LE (1998) Characterization of hydrogeologic units using matrix properties, Yucca Mountain, Nevada. US Geol Surv Water-Resour Invest Report 98:4243